Development/Plasticity/Repair

SPARC Regulates Microgliosis and Functional Recovery following Cortical Ischemia

Samantha M. Lloyd-Burton,[1] Elisa M. York,[1] Mohammad A. Anwar,[1] Adele J. Vincent,[2] and A. Jane Roskams[1]

[1]Department of Zoology, Life Sciences Institute and Brain Research Centre, University of British Columbia, Vancouver, BC, V6T 1Z3, Canada and [2]Menzies Research Institute, University of Tasmania, Hobart, TAS 7000, Australia

Secreted protein acidic rich in cysteine (SPARC) is a matricellular protein that modulates the activity of growth factors, cytokines, and extracellular matrix to play multiple roles in tissue development and repair, such as cellular adhesion, migration, and proliferation. Throughout the CNS, SPARC is highly localized in mature ramified microglia, but its role in microglia—in development or during response to disease or injury—is not understood. In the postnatal brain, immature amoeboid myeloid precursors only induce SPARC expression after they cease proliferation and migration, and transform into mature, ramified resting microglia. SPARC null/CX3CR1-GFP reporter mice reveal that SPARC regulates the distribution and branching of mature microglia, with significant differences between cortical gray and white matter in both controls and SPARC nulls. Following ischemic and excitotoxic lesion, reactive, hypertrophic microglia rapidly downregulate and release SPARC at the lesion, concomitant with reactive, hypertrophic perilesion astrocytes upregulating SPARC. After photothrombotic stroke in the forelimb sensorimotor cortex, SPARC nulls demonstrate enhanced microgliosis in and around the lesion site, which accompanies significantly enhanced functional recovery by 32 d after lesion. Microglia from SPARC nulls also intrinsically proliferate at a greater rate *in vitro*—an enhanced effect that can be rescued by the addition of exogenous SPARC. SPARC is thus a novel regulator of microglial proliferation and structure, and, in addition to regulating glioma progression, may play an important role in differently regulating the gray and white matter microglial responses to CNS lesion—and modulating behavioral recovery—after injury.

Introduction

The matricellular protein secreted protein acidic rich in cysteine (SPARC, osteonectin, BM-40) is largely restricted in the adult CNS to microglia and some subcortical astrocytes (Vincent et al., 2008). SPARC acts in a multimodal manner by regulating growth factor signaling, extracellular matrix (ECM) assembly, and cell-matrix interactions, enabling it to regulate processes important for tissue repair, such as cellular adhesion, migration, and proliferation (Brekken and Sage, 2001; Murphy-Ullrich, 2001). Consistent with mice lacking other matricellular proteins, SPARC-null mice have a subtle phenotype that is best revealed by challenge, for example, abnormal fibroblast migration during dermal wound healing (Basu et al., 2001; Bradshaw et al., 2002) and increased cardiac rupture following myocardial infarction (Schellings et al., 2009). Recently, matricellular proteins like SPARC and its ortholog, SPARC-like 1 (SC1, Hevin), have been implicated in critically important functions in the CNS, including regulation of synaptic stability (Jones et al., 2011; Kucukdereli et al., 2011) and cortical lamination (Gongidi et al., 2004).

SPARC is dynamically expressed by radial glia, astrocytes, and developing blood vessels during CNS development (Vincent et al., 2008), but is primarily found in "resting," ramified microglia in the adult CNS. Microglia perform a wide range of roles including immune surveillance, scavenging and phagocytosis, modulation of neurogenesis and synaptogenesis, and modulation of the microenvironment through secretion of cytokines (Ransohoff and Cardona, 2010). Following CNS lesion, microglia can have both potentially beneficial and detrimental actions, and therefore understanding how to regulate their spatiotemporal proliferation, migration, and activation after lesion could be critical to enhancing neural repair. After transplanting SPARC-null olfactory ensheathing cells (OECs) into a spinal cord injury, we earlier noted enhanced accumulation of macrophages and microglia at the lesion site, compared with the transplants of wild-type OECs (Au et al., 2007). This suggested that SPARC from OECs might control the local immune response, mirroring how SPARC regulates the immune response in other tissues (Sangaletti et al., 2005, 2011; Rempel et al., 2007).

To specifically test if SPARC can regulate neuroimmune responses independent of transplantation, here we used a focal

Received July 26, 2012; revised Jan. 22, 2013; accepted Jan. 25, 2013.

Author contributions: S.M.L.-B. and A.J.R. designed research; S.M.L.-B., E.M.Y., M.A.A., A.J.V., and A.J.R. performed research; A.J.R. contributed unpublished reagents/analytic tools; S.M.L.-B., E.M.Y., M.A.A., and A.J.R. analyzed data; S.M.L.-B., E.M.Y., and A.J.R. wrote the paper.

This work is supported by Canadian Institutes of Health Research MOP-89739, Michael Smith Foundation for Health Research Senior Scholar Award (A.J.R.), and MS Canada Postdoctoral Fellowship (S.M.L.-B.). We thank Kathryn Westendorf for technical assistance and expertise, and our awesome high school volunteer, Antigone (Tiggy) Valen, for her help in quantification, and Gavin Bock for assistance with behavioral analysis. We would also like to thank Khatereh Aminoltejari and Greg Silasi (from the lab of Dr. Tim Murphy, University of British Columbia) for their immense help in teaching us and troubleshooting rose bengal lesion and behavioral analysis. We would also like to thank Dr. Helene Sage for sharing reagents and insight into SPARC action, and Drs. Tim Murphy, Wolfram Tetzlaff, and Brian MacVicar for their collaboration and their insightful discussions of this manuscript.

The authors declare no competing financial interests.

Correspondence should be addressed to Dr. A. Jane Roskams, Room 3-309 Life Sciences Institute, University of British Columbia, 2350 Health Sciences Boulevard, Vancouver, BC V6T 1Z4, Canada. E-mail: roskams@zoology.ubc.ca.

DOI:10.1523/JNEUROSCI.3585-12.2013

 0270-6474/13/334468-14$15.00/0

photothrombotic cortical stroke lesion (Watson et al., 1985) and an NMDA-induced excitotoxic lesion. Ischemic stroke causes neuronal cell death and associated disability (Moskowitz et al., 2010), and the response to this and excitotoxic challenge involves multiple glia, including an inflammatory response by microglia and formation of a glial scar by activated astrocytes (Iadecola and Anrather, 2011). To better monitor microglial dynamics without relying on the detection of immune markers (that could change at different phases after lesion) we used double transgenic mice—SPARC-null mice with microglia that express green fluorescent protein (GFP) under the control of the Cx3cr1 promoter (Jung et al., 2000). We have established that SPARC in mature microglia is rapidly lost as microglia become activated after stroke and excitotoxic lesion, that exogenous SPARC is antiproliferative to microglia *in vitro*, and that following focal stroke *in vivo*, the enhanced microgliosis that occurs following stroke in the absence of SPARC promotes functional recovery.

Materials and Methods

Animals. Animal procedures were performed in accordance with the guidelines of the Canadian Council for Animal Care and the University of British Columbia Animal Care Committee. Mice that are homozygous for the CX3CR1-GFP targeted mutation (B6.129P-*Cx3cr1*^{tm1Litt}/J), SPARC-null mice (B6;129S-Sparc^{tm1Hwe}/J), and wild-type mice (B6129SF2/J) were obtained from The Jackson Laboratory. Equal numbers of male and female mice were used in this study.

Generation of Cx3Cr1-GFP SPARC-null mice. The CX3CR1-GFP targeted mutation and SPARC-null mice were first crossed to produce Cx3cr1+/GFP/SPARC+/− males and then back-crossed to SPARC-null females to produce Cx3cr1+/GFP/SPARC−/− or back-crossed to wild-type control females to produce Cx3cr1+/GFP/SPARC+/+ animals.

Genotyping. Animals were first genotyped by PCR to identify the SPARC nulls and SPARC wild types using primers MGSPARC-For 5′-GAT GAG GGT GGT CTG GCC CAG CCC TAG ATG CCC CTC AC-3′, NEOMYCIN-Rev 5′-GGT GTG CCC AGT CAT AGC CGA ATA GCC TCT CCA CCC AAG-3′, and MGSPARC-Rev 5′-CAC CCA CAC AGC TGG GGG TGA TCC AGA TAA GCC AAG-3′ followed by PCR for the Cx3cr1-GFP (previously recommended by The Jackson Laboratory) using primers oIMR3945 5′-TTC ACG TTC GGT CTG GTG GG-3′ (wild-type), oIMR3946 5′-GGT TCC TAG TGG AGC TAG GG-3′ (common to both wild-type and the Cx3cr1-GFP), and oIMR3947 5′-GAT CAC TCT CGG CAT GGA CG-3′ (Cx3cr1-GFP only).

Blinding of surgery and analysis. All mice were assigned a study number by the lab manager (who is in charge of mouse breeding and genotyping), and mixed together in equal numbers for different successive surgery days. Different surgery days also contained mice from different terminal time points (day 7 and day 32 analysis). Behavioral analysis was digitally recorded using these coded numbers, and mice were then reassigned numbers independently for analysis of behavior and pathology. Genotype of mice analyzed was subsequently decoded after independent evaluation of behavioral assays and pathology assessment.

Photothrombotic stroke surgery. The photothrombotic focal stroke method was performed as first described by Watson et al. (1985), and is usually modified to allow for differences in laser efficiency, and rose bengal delivery in different strains of mice. In brief, mice were anesthetized in an induction chamber ventilated with 5% isoflurane gas, and then transferred to a stereotaxic frame and maintained at 1.5% isoflurane using a nose mask. A midline incision of the scalp was made and a 1 × 1 mm region of the skull, 2.25 mm lateral and 1 mm caudal from bregma, was thinned to 50% of its original thickness. Two minutes after administration of rose bengal (1% solution dissolved in PBS, made fresh, 100 mg/kg, i.p.), a collimated green laser (532 nm wavelength at 17 mW) was used to illuminate the thinned area of skull for 20 min, to initiate photothrombosis. Three sutures were used to close the wound, and the mouse was monitored until it regained consciousness. Mice were monitored twice daily in the 48 h after surgery, and daily thereafter until experimental endpoint.

NMDA microinjection into olfactory bulb. Adult mice were anesthetized with xylazine (Rompun) and ketamine (0.5 mg of xylazine, 5 mg of ketamine, i.p.). The head was fixed to a stereotaxic frame with mouse face bars (David Kopf Instruments). An incision was made in the midline to expose the olfactory bulb (OB), and a hole was drilled into the skull just above the right OB (0.51 mm anterior, 0.10 mm lateral, 0.15 mm ventral from bregma). The needle of a 1 μl Hamilton syringe was lowered 1.5 mm into the right OB. Then 0.5 μl of NMDA (Sigma; 40 mM freshly prepared in 0.1 M PBS) was infused for 10 min, using a microinjection pump (UltraMicroPump; World Precision Instruments), and the needle was left in place for an additional 2 min. The incision was closed using Vetbond (3M Animal Care Products) and mice were allowed to recover from anesthesia. Sham animals received injections of vehicle only (0.1 M PBS).

Forelimb preference cylinder test. A modification (Vergara-Aragon et al., 2003; Porritt et al., 2012) of the cylinder or spontaneous forelimb test (Schallert et al., 2000) was performed 1 d before surgery (baseline) and at days 2, 8, 16, and 32 postsurgery. All mice were acclimatized to the cylinder tests before the commencement of stroke induction, and the measurements taken 24 h before stroke were used as their respective baseline. The time of day at which the test was performed remained consistent throughout. There are several variations of this test, but we chose to follow the protocol favored by the majority of recent researchers using a focal photothrombotic lesion (Porritt et al., 2012) or when assessing unilateral deficits (Vergara-Aragon et al., 2003). Each mouse was placed in a 15 cm diameter glass cylinder and videotaped for 10 min, with two mirrors placed at 60° behind the cylinder to ensure the camera captured a 360° view. This approach also gave us the opportunity to directly compare our baseline data and evaluation technique with that of our collaborator (Tim Murphy, University of British Columbia). The initial placement of forelimbs on the cylinder wall was scored for each rear. Simultaneous ipsilateral and contralateral forelimb touches (bilateral) were excluded from the evaluation of paw preference, but were considered to ensure the rate of placement was similar at different times within a given group of mice. Preferential paw placement was calculated by contralateral/contralateral + ipsilateral reaches ×100 (Vergara-Aragon et al., 2003) ($n = 6$ control, $n = 7$ SPARC null). Statistical analysis was performed using an unpaired *t* test with Welch's correction, which allows for the two groups possibly having unequal variances (accounting for measure of data spread).

Tissue processing. Mice were lethally injected with xylazine (Rompun) and ketamine (0.5 mg of xylazine, 5 mg of ketamine, i.p.) and transcardially perfused with ice-cold PBS followed by 4% paraformaldehyde (PFA) before the brains were dissected out and cryopreserved with successive 10 and 30% sucrose sinks in PBS for 24 h each. Brains were mounted coronally and frozen in Tissue Tek optimal cutting temperature compound in isopentane on dry ice. Frozen 14 μm sections were collected on Superfrost Plus slides and stored at −20°C. Free-floating 50 μm coronal sections were collected from adult brain and stored in PBS + 0.01% sodium azide at 4°C.

Immunohistochemistry of tissue. Tissue was permeabilized in 0.1% Triton X-100 (Sigma) for 30 min, washed in PBS, blocked in 4% normal serum for 20 min, and incubated with primary antibodies (see below) in 2% normal serum at 4°C for 16 h. Primary antibodies: goat anti-SPARC (1:125; R&D Systems) (Vincent et al., 2008), rabbit anti-Iba-1 (1:1000; Wako), rabbit anti-GFAP (1:750; Dako), rat anti-galectin 3 (1:500; Santa Cruz Biotechnology), rabbit anti-laminin (1:1000; Sigma), mouse anti-proliferating cell nucleic acid (PCNA; 1:5000; Sigma), and chicken anti-GFP (1:1000; Aves Labs). Detection used fluorescent secondary antibodies (Alexa Fluor 488 or 594; 1:200; Invitrogen) incubated for 1 h at room temperature, or by peroxidase chromogen reaction using biotinylated secondary antibodies (1:200), and Vectastain ABC kit and Vector VIP kits (Vector Laboratories). Nuclei were counterstained with 0.5 μg/ml 4′,6-diamidine-2-phenylindole dihydrochloride (DAPI; Boehringer Mannheim) and sections were mounted using Vectashield (Vector Laboratories) or ProLong Gold (Invitrogen). Isolectin-IB4 directly conjugated to Alexa 594 was included at the same time as secondary antibodies, where appropriate. For negative controls, primary antibodies were omitted or nonspecific primary antibodies used. Antigen unmasking for

PCNA immunofluorescence, was performed by heating sections for 10 min in 10 mM citrate buffer, pH 6.0, before the permeabilization step. If performing antigen unmasking, an anti-GFP antibody must be used to visualize endogenous GFP.

Culture of postnatal microglia. Microglia were derived from postnatal days 1–3 (P1–P3) mouse brains. Mice were decapitated and brains dissected out. Brains were placed in ice-cold HBSS (Invitrogen) with 1% P/S (penicillin-streptomycin; Invitrogen) on ice and bisected mid-sagittally, and the midbrain and olfactory bulbs were cut away with spring microscissors. The meninges were peeled away from the surface of the cortex before cortical sheets were chopped finely with a razor blade, incubated in 0.25% trypsin (Sigma) and 0.03% rat tail collagenase (Sigma) for 30 min at 37°C, and dissociated into a single-cell suspension by multiple passes through a P1000 tip. Suspensions were passed through a 40 μm filter, spun at 500 $\times$ *g* for 5 min, and plated into a T75 precoated for 1 h at room temperature with 0.05 mg/ml poly-L-lysine (Sigma) in DMEM (Invitrogen) containing 10% heat-inactivated fetal bovine serum (FBS) and 1% P/S. After 24 h all media and tissue was removed and fresh media was added. After 7 d one half of the media was replaced and cells were maintained as a mixed glia culture until day 14. At 14 d, microglia were removed from the mixed glial culture via a rotating shaker at 200 rpm for 45 min, and transferred to a new T75 or plated onto poly-L-lysine-coated glass coverslips.

Culture of adult microglia. Microglia were derived from adult (6–10 weeks) mouse brains. Stock Percoll (Sigma) was diluted 1:10 in sterile 10× PBS to yield 100% stock isotonic Percoll (SIP). One hundred percent SIP was then diluted in 1× PBS to yield 70 and 40% SIP. SIP solutions were brought to room temperature (RT) before use. Mice were lethally injected with xylazine (Rompun) and ketamine (0.5 mg of xylazine, 5 mg of ketamine, i.p.) and transcardially perfused with 25 ml of ice-cold PBS, before the brains were dissected out. Cortices were isolated, meninges removed, and tissue was chopped up with a razorblade before being subjected to mechanical dissociation using a Dounce homogenizer with loose fitting pestle. The cell suspension was then passed through an 80 μm cell strainer. Homogenates from two mice were resuspended in 5 ml of 70% SIP in a 50 ml conical tube and overlaid with 7 ml of 40% SIP and 5 ml of HBSS, followed by a 30 min centrifugation at 800 $\times$ g without braking. The mononuclear cell fraction was collected from the 40/70 interphase and the cells were washed twice, before resuspension in DMEM supplemented with 2 mM L-glutamine (Invitrogen), 1% P/S, and 10% FBS. Cells were plated at 1×10^5 /cm on poly-L-lysine-coated glass coverslips, in the presence of 10 ng/ml M-CSF.

Immunocytochemistry. Cells were plated onto poly-L-lysine-coated glass coverslips. They were fixed for immunocytochemistry by rinsing twice in 1× PBS for 5 min, followed by 10 min of fixation in 4% PFA, two rinses for 5 min each in 1× PBS, and storage in 0.05% azide in 1× PBS. Cells were permeabilized in 0.1% Triton X-100 for 30 min, washed three times, and blocked with 4% normal donkey serum for 1 h at room temperature. Cells were incubated with primary antibodies in 2% normal serum for 1 h at room temperature or 16 h at 4°C. Microglia were immunolabeled with rabbit anti-Iba-1 (1:1000; Wako) or rabbit anti-NFκB (1:100; Santa Cruz Biotechnology). Detection used fluorescent secondary antibodies (Alexa Fluor 488 or 594; 1:200; Invitrogen) incubated for 1 h at room temperature in 2% normal serum. Isolectin-IB4 directly conjugated to Alexa 594 was included at the same time as secondary antibodies, where appropriate. Nuclei were counterstained with 0.5 μg/ml DAPI (Sigma) and coverslips were mounted using ProLong Gold (Invitrogen).

Assessment of microglial proliferation. For assessment of microglial proliferation, adult microglial cultures growing on poly-L-lysine-coated glass coverslips were used at 4 days *in vitro* (DIV). Fresh DMEM with 2% FBS was applied for 18 h before supplementation of media with recombinant mouse SPARC (1–10 ng/ml; R&D Systems) and 10 μM 5-ethynyl-2′-deoxyuridine (EdU; Invitrogen). Twenty-four hours later, fresh DMEM with 10% FBS was applied and cells were allowed to recover for a further 24 h before fixation and detection of EdU. Cells were fixed as outlined above, and EdU was detected using an Invitrogen Alexa Fluor 488 Click-IT kit, according to the manufacturer's protocol. Microglial identity was confirmed with Isolectin-IB4 labeling. Nuclei were counterstained with 0.5 μg/ml DAPI (Sigma) and coverslips were mounted using ProLong Gold (Invitrogen).

Image capture. Images were captured using an Axioplan 2 Imaging epifluorescent microscope (Zeiss) with Zeiss Axiovision software or a Fluoview FV1000 laser scanning confocal microscope. Images were corrected for contrast and brightness using Photoshop CS3 software (Adobe Systems). For quantification, all images were captured with uniform settings, and no post processing was performed.

Quantification of microglia in vitro. For quantification of microglial cell numbers at DIV 8, 10 micrographs at 10× magnification were collected for each 12 mm coverslip ($n = 3$). Microglial purity was 97%, as determined by isolectin IB4 labeling. DAPI-positive nuclei were counted using ImageJ and converted to cells per square millimeter. Data were subjected to a Student's *t* test for significance.

For quantification of proliferation, five micrographs at 10 × magnification were collected for each 12 mm coverslip ($n = 3$ separate cell culture preps). DAPI and EdU-positive nuclei were counted using ImageJ and results expressed as number of EdU-positive nuclei per total area. Data were subjected to a two-way ANOVA with Bonferroni post-test.

Quantification of microglial density in vivo. Six 20× fields of view of predetermined locations throughout the cortical gray matter of coronal sections were captured. Three cortical planes were sampled to cover rostral, mid, and caudal cortex. Sections from different animals ($n = 3$–4) were matched according to stereological landmarks. Following immunofluorescent detection of Iba-1, individual microglia were counted using the ImageJ Count feature. Counts were converted to microglia per square millimeter and averaged over each animal. Data were subjected to an unpaired Student's *t* test for significance.

Quantification of microglial morphology in vivo. Four serial coronal sections per mouse ($n = 3$) through the midline of the lesion were prepared for the following analysis. Six *z*-stacked fields of view at predetermined locations in the cortex and corpus callosum on the uninjured contralateral hemisphere per brain section were captured using a 63× objective on an Axioplan 2 Imaging epifluorescent microscope (Zeiss). *Z*-stacks were subjected to iterative deconvolution using the Zeiss Axiovision deconvolution module, and then flattened using a maximum intensity projection. Three gray matter and three white matter microglia per serial section were thresholded in ImageJ to create a binary image, with consistent settings used throughout. Process outgrowth was measured using the ImageJ Skeletonize and Histogram features and the pixel value converted to total micrometers. Multiple parameters were analyzed using the ImageJ Analyze Skeleton plug-in. Data were subjected to an unpaired Student's *t* test for significance.

Infarct volume measurement

For all Nissl staining analysis, we followed standard cresyl violet staining protocols used for lesion volume assessment, and also compared them with the distribution of DAPI-stained nuclei. For mice analyzed at 7 d post injury (DPI), every fourth slide (minimum of 10 sections) through the lesion was tested to create an accurate sample of the injury, and stained by immunofluorescence for microglia (Iba-1 or GFP) and astrocytes (GFAP). Area of injury was outlined and measured using ImageJ software (Zhang et al., 2010), and compared with cortical volume on the contralateral side within the same section. Thirty-two days after stroke, every second slide was Nissl stained throughout the lesion and imaged with bright-field microscopy, in addition to imaging and analyzing the area occupied by GFP+ microglia in the CX3CR1-GFP transgenic mouse crosses. The area of injury was outlined and measured using ImageJ software (Zhang et al., 2010) and the volume of the lesion was determined with the following formula: mean area of lesion × distance between sections × number of sections, as described by Clark et al. (2008).

Quantification of enhanced GFP and galectin-3 fluorescence. Serial sections through the midline of the lesion were prepared for analysis, and the maximal planar area of fluorescence was assayed ($n = 5$). Four 10× micrographs were collected for each section, covering a total area of 1.5 × 1 mm around the lesion, with the full thickness of the cortex included. Images were merged in Photoshop, using the Photomerge (reposition only, no blending) feature. Images were then thresholded in ImageJ to

create a binary image, with consistent settings used throughout. Data are represented as number of positive pixels in a constant area, and subjected to an unpaired Student's *t* test for significance.

Quantification of PCNA-positive cells. Two serial sections through the midline of the lesion were analyzed for each brain ($n = 3$). Four 10× micrographs were collected for each section, covering a total area of 1.5 × 1 mm around the lesion, with the full thickness of the cortex included. Images were merged in Photoshop, using the Photomerge (reposition only, no blending) feature. Images were then thresholded in ImageJ to create a binary image, and PCNA-positive nuclei were counted using the ImageJ Analyze Particles tool. Data were analyzed using an unpaired Student's *t* test for significance.

Results

SPARC is expressed by mature ramified microglia throughout the brain

Microglial cells, the resident immune cells of the CNS, are of myeloid origin. They are derived from progenitors in the yolk sac, and enter the CNS during early embryonic development (Chan et al., 2007). In the postnatal CNS, microglial precursors proliferate in multiple sites, termed "fountains of microglia," including the lateral ventricle (Chan et al., 2007). In the P6 cerebral cortex, SPARC– detected using an antibody that does not identify SPARC in the CNS of SPARC nulls (Vincent et al., 2008; Lloyd-Burton and Roskams, 2012)—is not expressed by amoeboid, migratory Iba-1-positive microglial precursors at the lateral ventricle (Fig. 1*A*). SPARC is instead primarily expressed by residual radial glial cells (Vincent et al., 2008). At P9, the majority of microglia are migrating throughout the brain and do not express SPARC, whereas in some regions, they are beginning to adopt a more mature, ramified morphology (Fig. 1*B*). At P12, when migration is almost complete, SPARC expression can be readily detected in fully mature, resident ramified microglia (Fig. 1*C*). This is most obvious in the cortical parenchyma, where SPARC is largely absent from Iba-1-positive cells at P6 and P9, but universally expressed from P12 (Fig. 1*D–F*). An identical spatiotemporal pattern of microglial SPARC expression was obtained when microglia were visualized with isolectin IB4 (data not shown). Microglia are heterogeneous cells, displaying regional phenotypic variation, yet the expression of SPARC by microglia appears to be universal throughout the brain. In the cerebral cortex and corpus callosum, SPARC is expressed only by microglia (Fig. 1*G*,*H*). In other regions of the CNS, including the hippocampus (Fig. 1*I*), cerebellum (Fig. 1*J*), and thalamus (Fig. 1*K*), SPARC is variably expressed in postnatal development by other glia (e.g., astrocytes and Bergmann glia) (Vincent et al., 2008), yet microglial expression remains constant. In contrast, Iba-1-positive resting macrophages in the choroid plexus do not express detectable levels of SPARC (Fig. 1*L*).

Glial SPARC expression is altered following photothrombotic cortical stroke and excitotoxic lesion of the OB

In order to test if SPARC may contribute to both glial and neuroimmune response to lesion, we used immunohistochemical and immunofluorescence detection to establish the spatiotemporal dynamics of SPARC expression following a focal, noninvasive photothrombotic stroke lesion. At two days post insult, SPARC protein is not found in the ischemic lesion core, and no change in expression is observed in the perilesion zone (Fig. 2*A*). From 1 week post insult, SPARC immunoreactivity is increased robustly both in the lesion core and in the perilesion zone (Fig. 2*B*). This elevated expression is maintained until at least four weeks post insult (Fig. 2*C*,*D*). At 1 week post insult, the infarct core is populated with Iba-1-positive amoeboid phagocytic mixtures of microglia and macrophages. The perilesion zone contains a high density of activated hypertrophic microglia, with elevated Iba-1 levels (Fig. 2*E*). In contrast to ramified microglia in the contralateral cerebral cortex (Fig. 2*F*), the vast majority of hypertrophic microglia in the perilesion zone no longer express SPARC (Fig. 2*G*). Conversely, SPARC expression is normally absent from cortical astrocytes (Fig. 2*H*,*I*), but is upregulated in hypertrophic reactive astrocytes in the perilesion zone (Fig. 2*J*, open arrowhead). In addition, SPARC expression is detected in cells associated with laminin-positive blood vessels in the injured cerebral cortex (Fig. 2*K–M*).

In order to establish whether loss of SPARC expression in microglia are specific to ischemic stroke, or represent a more universal event accompanying microglial activation following different CNS lesions, we applied the same analysis to an excitotoxic lesion of the OB. In the uninjured OB (Fig. 3*A–F*), SPARC is expressed by ramified microglia in all cell layers, other than the outer nerve fiber layer, where it is also expressed by OECs (Au et al., 2007). Infusion of NMDA into the OB leads to excitotoxic death of subsets of glutamatergic OB neurons, and initiates a full gliotic response (Sultan-Styne et al., 2009). This excitotoxic lesion results in the rapid activation of microglia, which upregulate Iba-1 and become hypertrophic within 24 h after NMDA infusion (Fig. 3*G–L*). Consistent with microglial activation following photothrombotic stroke, reactive hypertrophic microglia in the NMDA-lesioned OB rapidly secrete and downregulate SPARC as they become activated and mobilized to phagocytize apoptotic neurons.

Microglial morphology is drastically altered in the SPARC-null CNS

Although SPARC is clearly specifically enriched in mature microglia, does this have any functional consequences at rest or following lesion? To better visualize how SPARC may directly impact the response of microglia to stroke lesion (and remove the variables that may accompany immunofluorescent quantification), we used transgenic mice where enhanced GFP (EGFP) is expressed in resident microglia, driven by the *Cx3cr1* promoter (Jung et al., 2000; Nimmerjahn et al., 2005). These mice were crossed with SPARC-null mice to produce offspring that were heterozygous for GFP-CX3CR1 and homozygous SPARC null. In the uninjured adult SPARC-null CNS at low magnification, Iba-1 intensity initially appeared similar to control mice (Fig. 4*A*,*B*). We also performed flow cytometric analysis for Cd11b and CD45 in microglia from SPARC-null and control mice and found there were no major differences in the expression of these microglia markers (data not shown), nor a change in the overall yield of microglia in the brain. However, when we combined the detection of Iba-1 with GFP, it is clear that the cortical gray matter density of Iba-1-positive microglial cell bodies (the main antigen normally used to detect mature CNS microglia) is significantly higher, whereas it is significantly lower in the white matter of the SPARC null, compared with controls (Fig. 4*C*). In addition, when visualizing SPARC-null microglia with GFP in the GFP-CX3CR1/SPARC-null mouse at high magnification, microglial morphology appeared to be significantly more complex and varied in the null than could be detected with Iba-1 immunofluorescence. To directly test this, we performed detailed morphological analysis of endogenous GFP distribution in CX3CR1-GFP microglia in the cortex of both SPARC-null and control mice (Fig. 4*D–I*). *Z*-stacks of individual microglia, sampled from equivalent sites in the gray and white matter, were deconvolved, flattened (Fig. 4*D*), skeletonized (Fig. 4*E*), and analyzed for total process

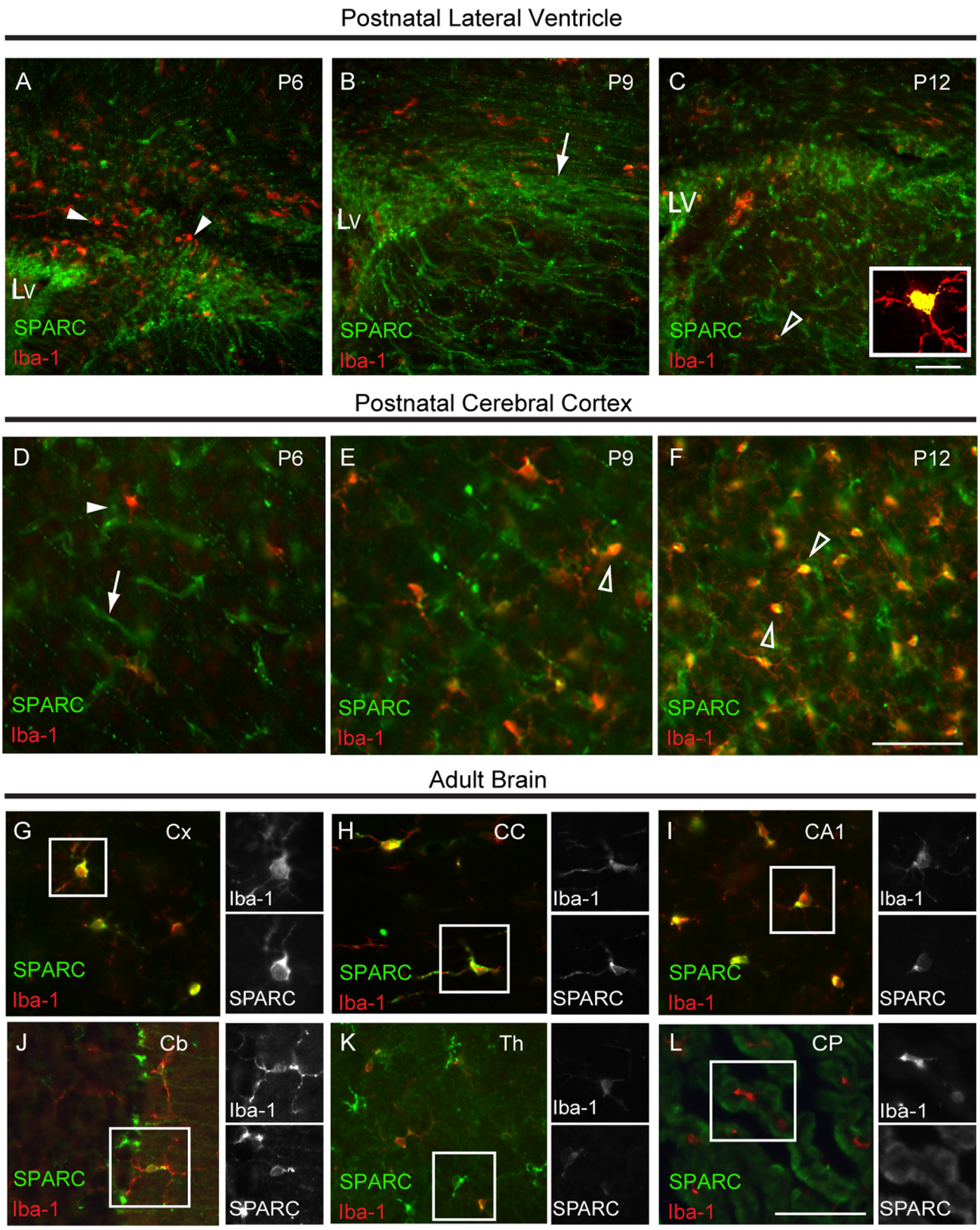

Figure 1. SPARC is expressed by mature ramified microglia in the brain. ***A***, At P6 migratory, amoeboid developing microglia expressing Iaba-1 (red, closed arrowhead) enter the brain parenchyma and are detected as clusters around the lateral ventricle (LV) that rarely coexpress SPARC (green), which is enriched in radial glial processes (green). ***B***, ***C***, From P9 to P12, microglia migrate away from the LV into the brain, differentiate into a ramified morphology, and begin to express SPARC (open arrowhead; inset). ***D***, In the P6 cerebral cortex, SPARC is primarily expressed in radial glia processes (green, arrow) and is absent from Iba-1-expressing immature microglia (arrowhead, red). ***E***, ***F***, From P9 to P12, microglia invade the cortex and become ramified, and by P12, SPARC is coexpressed with Iba-1 (yellow-orange, open arrowheads) in all cortical microglia. In the adult brain, SPARC is expressed by Iba-1-positive microglia in all regions, including the cerebral cortex (***G***; Cx); the corpus callosum (***H***; CC); the CA1 region of the hippocampus (CA1; ***I***); the cerebellum (***J***; Cb), where SPARC is also detected in Bergmann glia (Iba-1-negative); and the thalamus (***K***; Th), one of the few adult regions where Iba-1-negative astrocytes express SPARC (green). ***L***, SPARC is not detected in Iba-1-positive macrophages in the adult choroid plexus (CP). Scale bars: 20 μm.

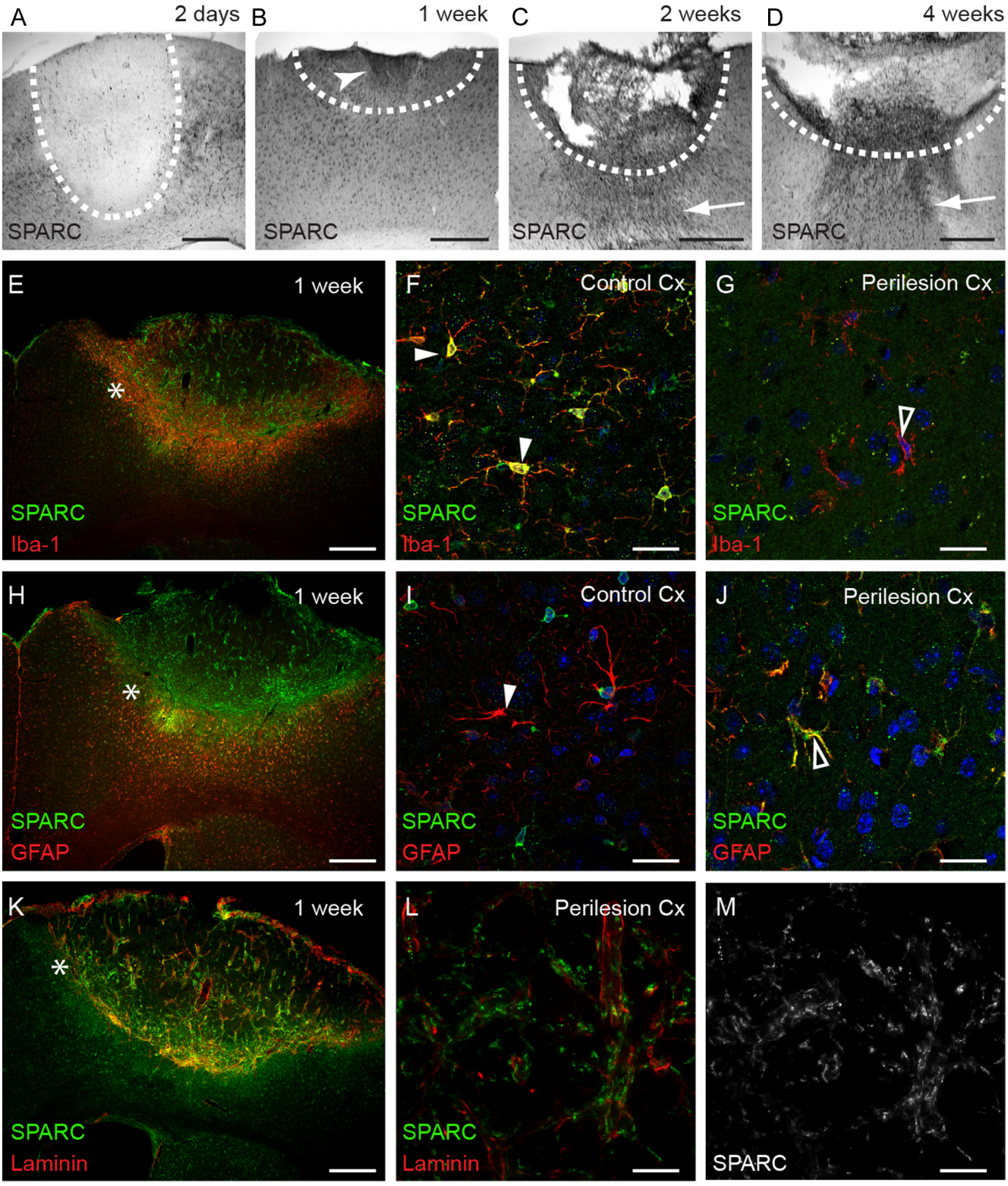

Figure 2. SPARC is downregulated in microglia and upregulated in astrocytes following photothrombotic stroke. ***A–D***, Using VIP immunohistochemistry, SPARC is initially absent from the initial infarct (***A***; demarcated by dotted line) but is readily detected at all levels of the lesion core and perilesion zone at 1 week after photothrombotic stroke (***B***; rostral edge of lesion shown, arrowhead), and is elevated at the center of the lesion and cells migrating to the lesion (***C***, ***D***; arrows) until at least 4 weeks post injury. At 1 week post lesion (***E***), SPARC appears diffusely throughout the lesion core, and although SPARC (green) colocalizes (yellow) in Iba-1-expressing (red) ramified microglia (***F***; arrowhead) in the uninjured cortex, SPARC is not in activated hypertrophic microglia (***G***; red, open arrowhead) in the perilesion zone (region, asterisk in ***E***, ***H***, ***K***). ***I***, SPARC is normally undetectable in GFAP-expressing (red) cortical astrocytes (arrowhead), but is upregulated (***H***, ***J***) in hypertrophic astrocytes at the outer margin of the perilesion zone (open arrowhead). ***K–M***, SPARC (green/white) is also upregulated on cells closely associated with laminin-expressing (red) blood vessels in the lesion core and perilesion zone. Scale bars: ***A–D***, ***E***, ***J***, ***K***, ***H***, 100 μm; ***F***, ***G***, ***I***, ***J***, ***L–M***, 10 μm.

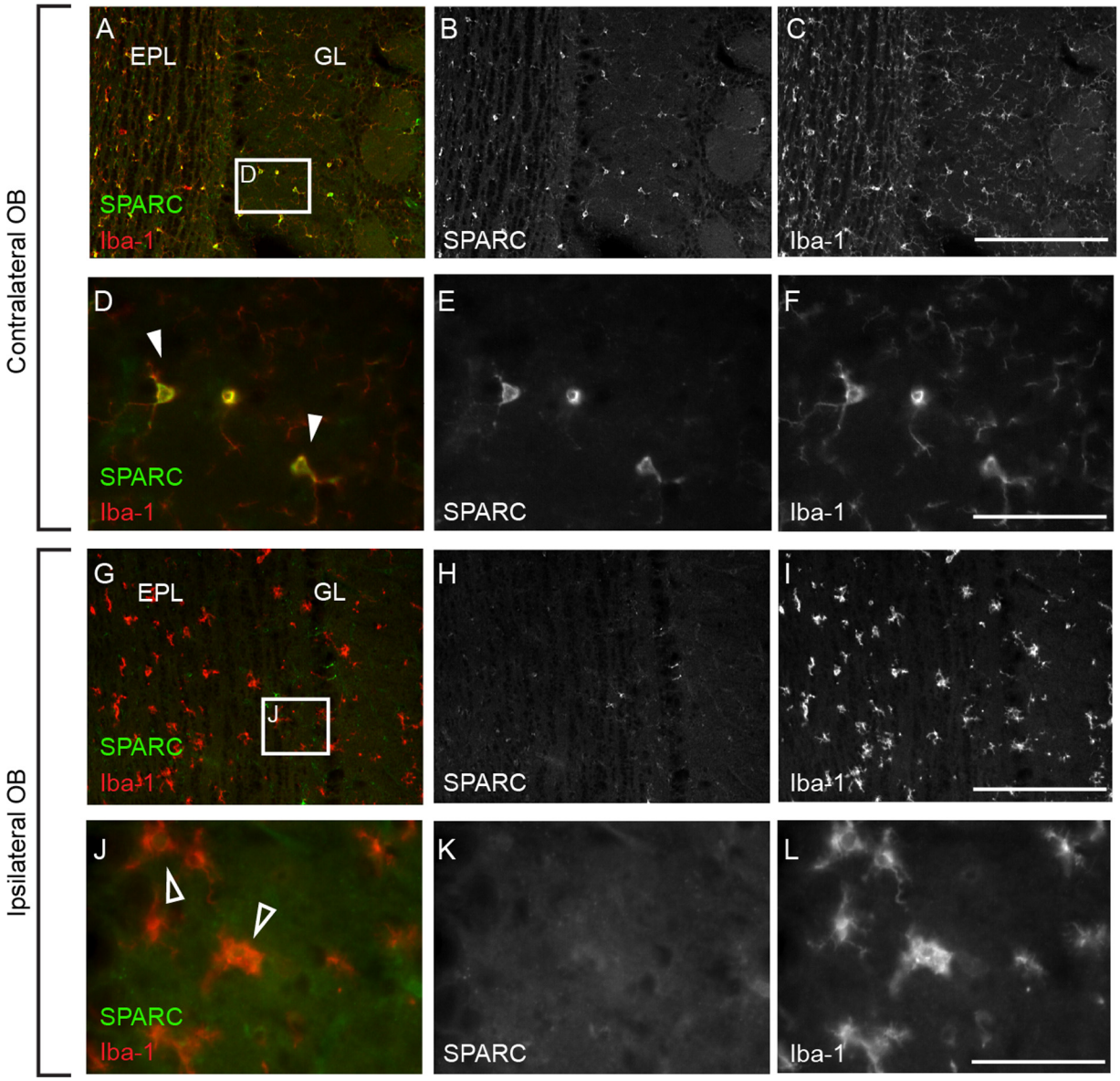

Figure 3. SPARC is lost in reactive microglia following NMDA excitotoxic lesion of the OB. ***A–C***, In the contralateral unlesioned OB (***B***) SPARC (green) is coexpressed by ramified Iba-1-expressing (red) microglia in all neuronal layers of the OB, with the glomerular layer (GL) and external plexiform (EPL) layer shown. ***D–F***, High magnification of boxed area in ***A***, showing SPARC coexpressed by Iba-1-expressing ramified microglia (arrowheads). ***G–I***, Twenty-four hours after infusion of NMDA into the ipsilateral OB, at the peak of excitotoxic neuronal death, Iba-1-positive microglia become hypertrophic and reactive (***I***), at which point SPARC immunoreactivity is no longer detectable in microglia (***H***). ***J–L***, High magnification of boxed area in ***G***, showing SPARC-negative hypertrophic microglia (open arrowheads). Scale bars: (in ***C***) ***A–C***, 100 μm; (in ***I***) ***G–I***, 100 μm; (in ***F***) ***D–F***, 20 μm; (in ***L***) ***J–L***, 20 μm.

outgrowth and branching (Fig. 4*F–I*). Microglial processes in both the SPARC-null gray matter and white matter are significantly longer compared with the wild-type reporter mice (Fig. 4*J*). In addition, microglial processes in the SPARC-null white matter showed significantly increased branching relative to the controls (Fig. 4*K*).

SPARC-null mice do not develop different size lesions in response to photothrombotic stroke

At the onset of this project, early experiments (where we did not shave the skull substantially) indicated that SPARC-null mice may develop variable, larger lesions in response to photothrombosis than control mice, with decreased survival. We concluded that this might be because the lack of SPARC may cause thinner skull density and stimulate a greater response to rose bengal in the same time window of laser exposure, as control. To counteract this, we modified our lesion approach to first shave a skull window to the same thickness (measured by degree of translucence), and use a less intense laser for longer time periods, yielding a small but reproducible lesion. However, given that resting microglia also appear biologically different (Fig. 4), and participate in the spread of lesion response, we also monitored lesion volume changes and lesion location using multiple approaches at two key time points after lesion–7 and 32 d. We detected early changes in lesion size by using a combination of astrocyte (GFAP) and microglial (Iba-1 or GFP) immunoreactivity (Fig. 5*A–E*) to delineate lesion boundaries, every 100 μm throughout the lesion. In addition, for 32 d analysis, sections at similar intervals were Nissl stained with cresyl violet to give two independent readings of lesion volumes throughout the lesion, which gave a similar distribution to intensely DAPI-stained nuclei (Fig. 5 *B*, *D*). The rostrocaudal lesion boundaries and lesion "core" were highlighted

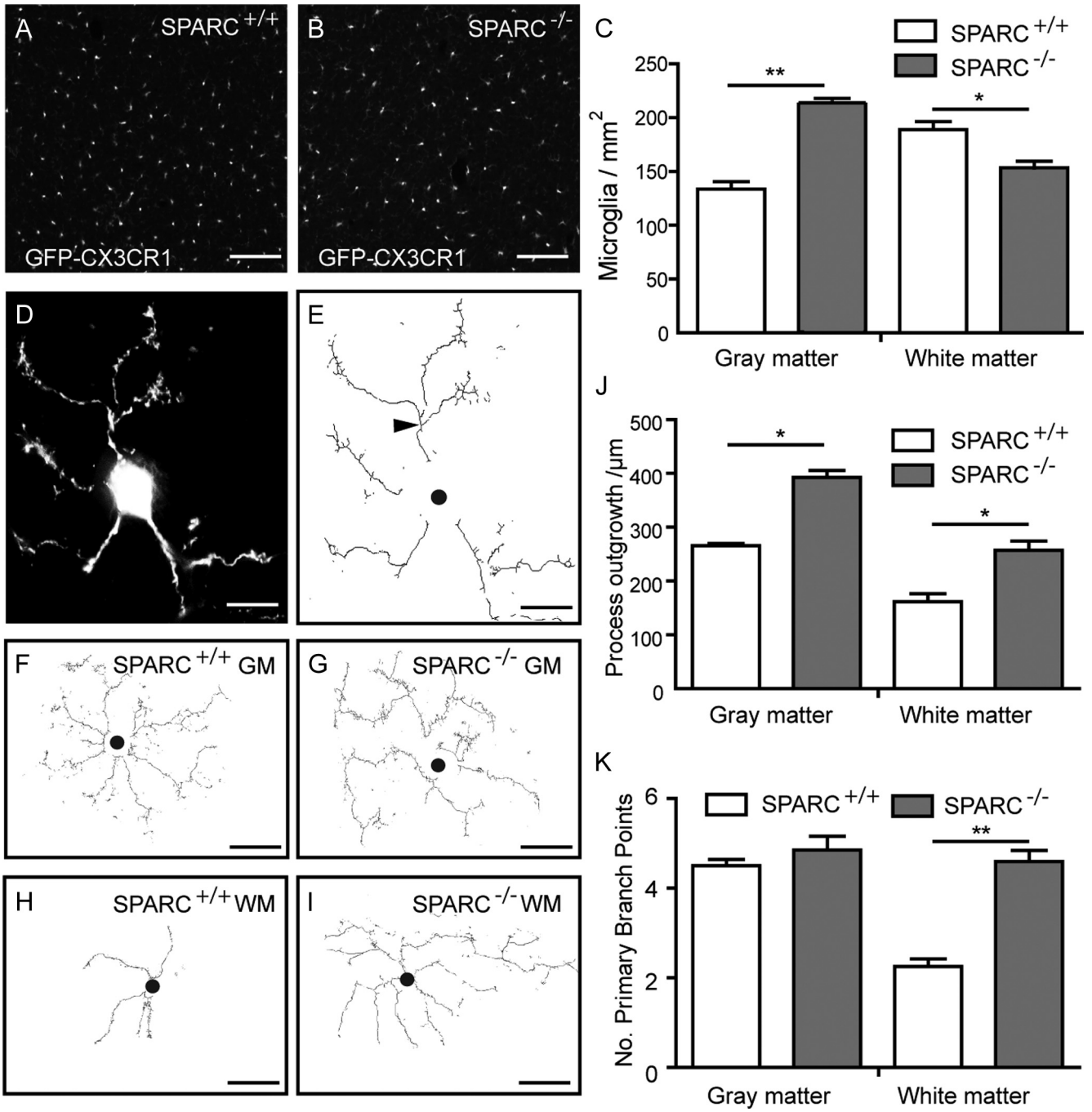

Figure 4. The absence of SPARC differentially regulates microglial expansion, process length, and branching in cortical gray and white matter in the uninjured SPARC-null cerebral cortex. ***A***, ***B***, GFP-expressing ramified microglia are evenly distributed, but Iba-1-positive cells (***C***) are more dense ($n = 3$) in SPARC nulls than control (+/+) ($p < 0.01$) and significantly less dense in the white matter of the corpus callosum ($p < 0.05$) compared with control mice. ***D***, Microglial morphology was analyzed by visualizing 3D deconvolved images of GFP+ microglia in SPARC null/CX3CR1-GFP double transgenic mice and skeletonizing to analyze for process outgrowth (microns per cell) and number of primary branch points (***E***, arrowhead). ***F–I***, SPARC-null microglia in the gray matter (***G***; GM) and white matter (***I***; WM) have increased process outgrowth (***J***; $p < 0.05$, Student's *t* test) and, in white matter, have more primary branch points (***K***; $p < 0.01$) than control microglia.

(Fig. 5 *A*, *G*) by microglial distribution (Iba-1/GFP), and location determined using anatomical landmarks at the lateral ventricle, anterior commissure, and hippocampus, visualized by DAPI staining. SPARC-null lesions extended from −0.342 to −0.504 mm from bregma at 7 DPI compared with controls (+0.144 to −0.808 mm). Lesions condensed by 32 DPI (Fig. 5*F*), where nulls extended from −0.507 to −1.24 mm, compared with −0.850 to −1.393 mm for controls. Although lesions in both groups varied within this (with a trend to larger initial lesions in many SPARC-null mice), comprehensive assessment of lesion volume using multiple markers at both 7 and 32 d after injury yielded no significant difference (Fig. 5*F*) in between SPARC-null and control mice.

SPARC-null mice show increased microgliosis and enhanced functional recovery after photothrombotic stroke

Given the increased density and altered morphology of microglia in the double transgenic, it became clear that we needed to test if there were functional consequences to this altered distribution and morphology. During the process of activation within the

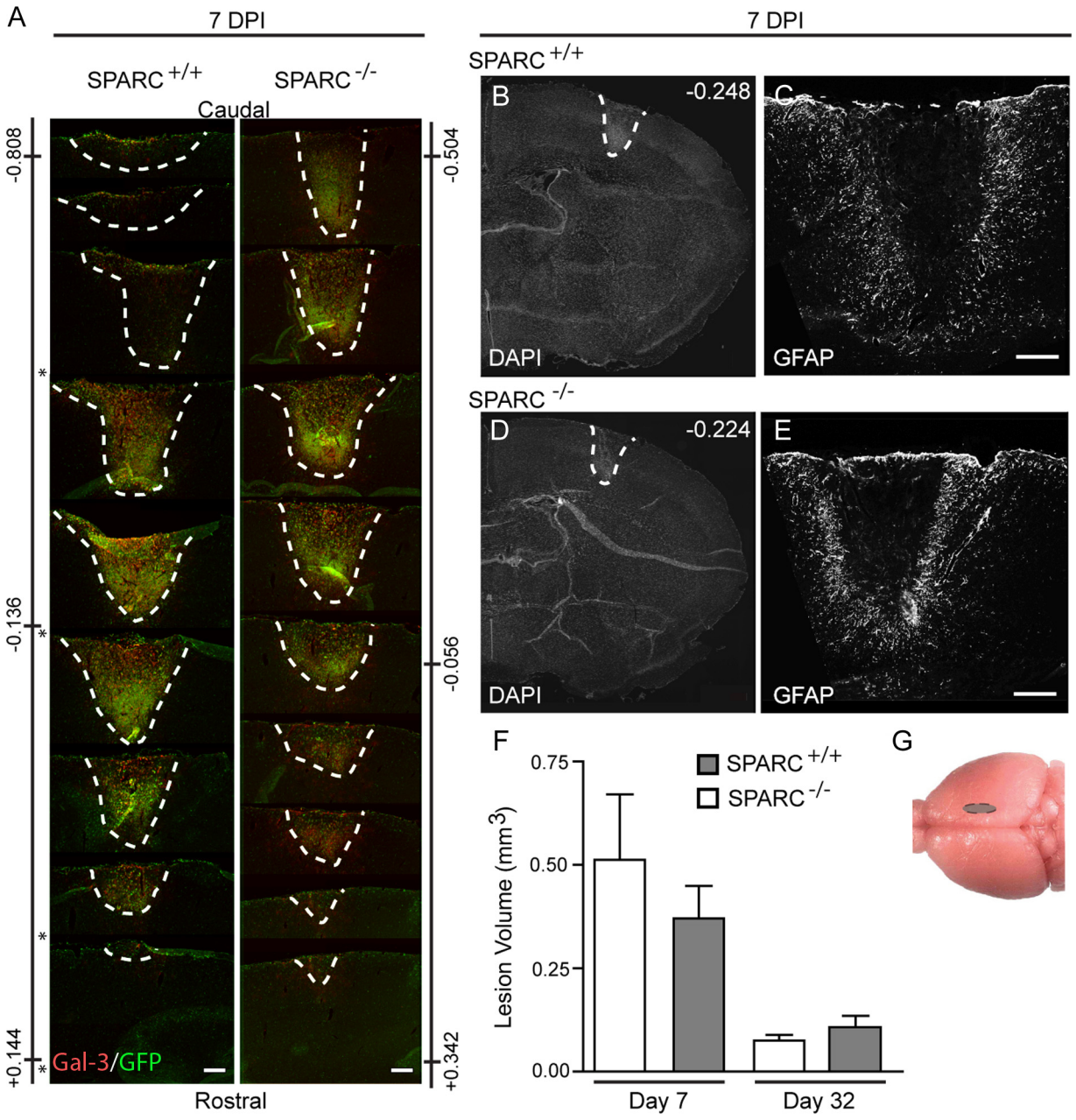

Figure 5. SPARC-null mice do not develop smaller lesions following photothrombotic stroke. Seven days after inducing photothrombotic stroke (7 DPI). ***A***, Using immunofluorescence for GFP or Iba-1 (green) and Gal-3 (red) in staggered sections through the lesion site reveals a similar location and extent of lesion in SPARC nulls (−/−) and controls (+/+). (Asterisk indicates sections that were used in calculations, but removed for figure construction). Black vertical bars indicate distance from bregma. The lesion site could be clearly delineated with a combination of DAPI+ nuclei (***B***, ***D***) GFAP (***C***, ***E***) in the astrogliotic lesion penumbra. ***F***, At 7DPI, lesion volumes in both SPARC-null (−/−) and control (+/+) mice were variable but not significantly different, with lesion volume shrinking in both genotypes by 32 DPI, but still not significantly different from each other. ***G***, Indicates the cortical area within which all lesions were located. Scale bars: ***A***, 100 mm; ***C***, ***E***, 60 mm.

CNS, microglia undergo extensive and rapid morphological and biochemical changes (Figs. 1–3), including upregulation of Iba-1 and galectin-3 (Gal-3). Gal-3 is a 30 kDa β-galactosidase-binding lectin that is upregulated by reactive microglia and macrophages following ischemia (Walther et al., 2000; Yan et al., 2009). Gal-3 is not detected in ramified microglia in the uninjured cerebral cortex (Fig. 6*A*). In the perilesion zone at 7 d after photothrombotic stroke, a small proportion of reactive hypertrophic microglia begin to express Gal-3 (Fig. 6*B*), whereas in the infarct core, all amoeboid (phagocytic) microglia and macrophages strongly express Gal-3 (Fig. 6*C*). Gal-3 is thus considered a marker of the most highly activated microglia/macrophages in these kinds of CNS lesions. By this measure, at 7 DPI, microgliosis is significantly greater in the SPARC null (Fig. 6 *G–I*) compared with the wild type (Fig. 6 *D–F*), when assessed both by the distribution of GFP-CX3CR1 cells and by Gal-3 immunoreactivity (Fig. 6*J*). Functional recovery of paw preference was also assessed using a forelimb preference cylinder test (Schallert et al., 2000). Both wild-type and SPARC-null mice showed a similar degree of loss of contralateral limb sensorimotor function immediately after inducing photothrombotic stroke (Fig. 6*K*). From 7 d post ischemia, however, SPARC-null mice appeared to progressively demonstrate greater functional recovery (contralateral paw use) than control mice, that is significant by 32 d ($n = 7/6$, $p < 0.01$), when they achieved a contralateral paw placement rate similar to unlesioned mice.

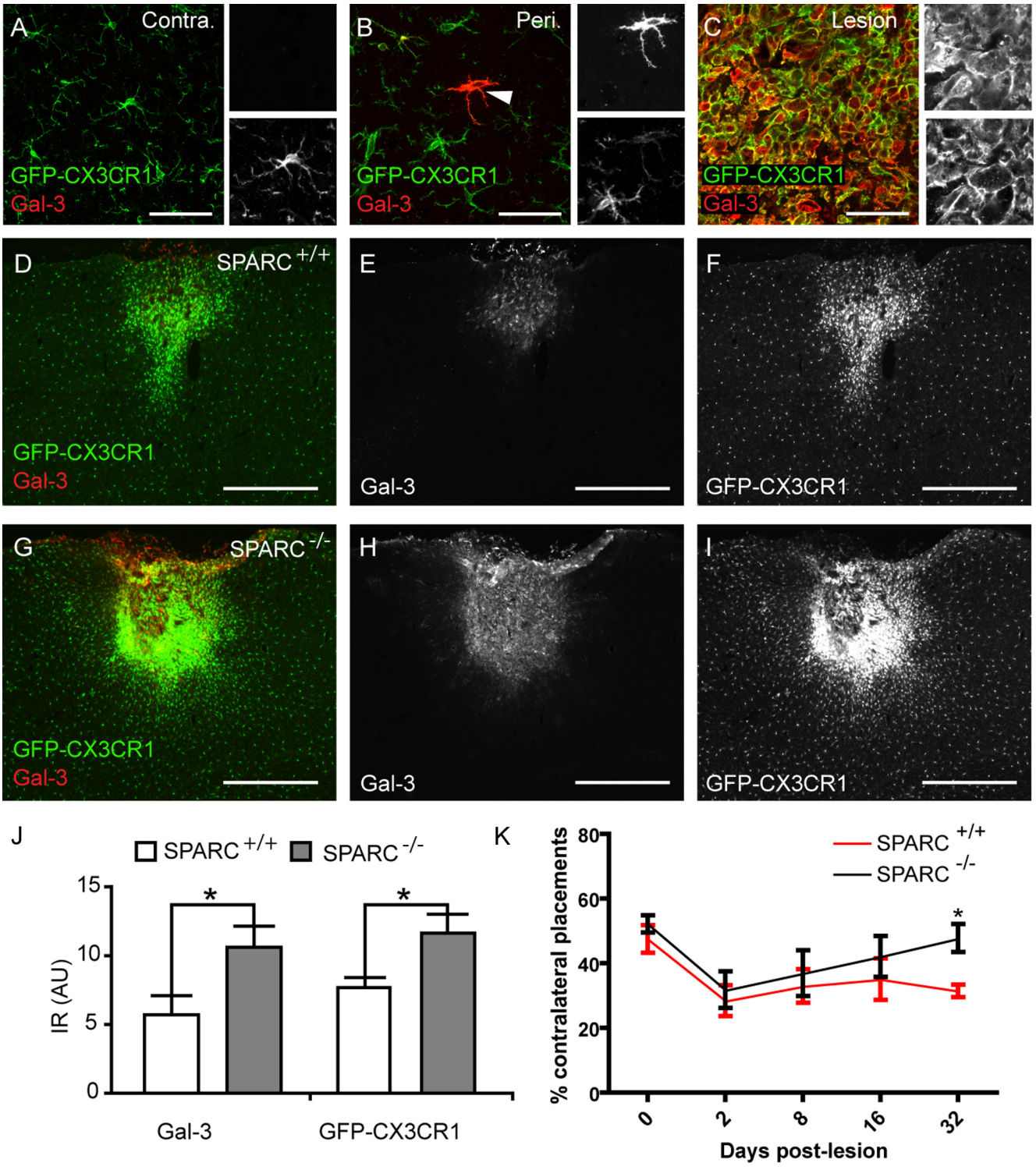

Figure 6. In SPARC nulls, microgliosis is increased and functional recovery is enhanced, following photothrombotic stroke. ***A***, ***B***, Seven days after photothrombotic stroke lesion, Gal-3 (red, used to indicate a high level of microglial activation) is not expressed by GFP-expressing (green) ramified microglia in the contralateral cortex (***A***; detail in insets), but is (***B***) expressed by a small proportion of hypertrophic activated microglia in the perilesion zone (peri), and is expressed by all amoeboid GFP-CX3CR1-positive cells in the lesion core (***C***). ***D–F***, In CX3CR1-GFP/SPARC control mice 1 week after surgery, both Gal-3 immunoreactivity and GFP-CX3CR1 signal are increased in the lesion core (images are representative maximal lesion core cross section). ***G–I***, In SPARC nulls, Gal-3-expressing cells and GFP-expressing cells in the lesion core and prelesion area appear to be significantly enhanced. ***J***, Gal-3 immunoreactivity (IR) and GFP-CX3CR1 normalized detection are significantly increased in the SPARC-null CNS relative to the wild-type (assayed area 1.5 × 1 mm centered on lesion as shown in ***D*** and ***G***; $n = 6–7$, $p < 0.05$ in both cases). ***K***, In the forelimb preference cylinder test, both SPARC-null and control mice showed a decrease in contralateral forelimb function following photothrombotic lesion to the forelimb sensorimotor cortex. SPARC-null mice demonstrated increased functional recovery by 32 d ($p < 0.01$, Student's *t* test with Welch's correction), SEM. Scale bars: ***A–C***, 40 μm; ***D–I***, 500 μm.

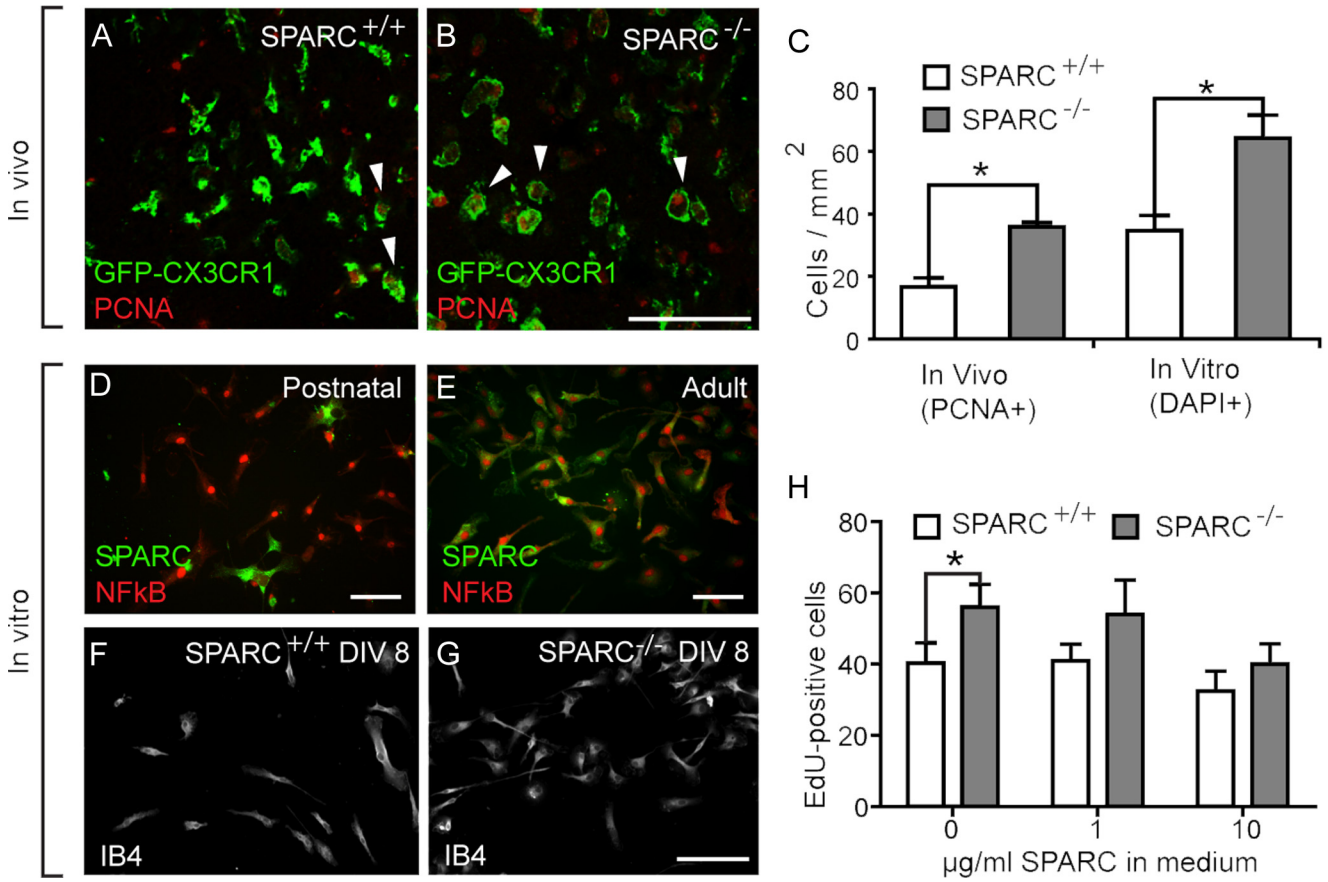

Figure 7. SPARC inhibits microglial proliferation *in vivo* and *in vitro*. Two days following photothrombotic stroke surgery, cortical microglia adjacent to the lesion in SPARC controls (***A***) become activated (more amoeboid) and proliferate (coexpress proliferating cell nuclear antigen, PCNA; red, arrowheads), a response which appears enhanced at this early stage lesion in the (***B***) SPARC null. ***C***, Proliferation of microglia, assessed by coexpression of PCNA with GFP-CX3CR1, is significantly increased in the SPARC-null cerebral cortex (images are representative; assayed area 1.5 × 1 mm centered on lesion; $p < 0.05$) relative to the wild-type controls. ***D***, SPARC is not expressed *in vitro* by partially activated NFκB-expressing microglia derived from postnatal mixed glial cultures, but is expressed *in vitro* by the majority of (***E***) adult-derived microglia. ***F–H***, Microglial cultures derived from SPARC-null adult mice are significantly higher in density after DIV 8, when compared with wild-type microglia. ***H***, SPARC-null adult-derived microglia proliferate at a significantly greater rate than wild-type microglia, as assessed by thymidine analog (EdU) uptake over 48 h. This effect is diminished by addition of exogenous SPARC to the culture media. Scale bars: 20 μm. All error bars are SEM.

Absence of SPARC leads to increased microglial proliferation *in vivo* and *in vitro*

Following photothrombotic stroke, microgliosis (defined as the accumulation of microglia at the lesion site following injury) is enhanced in the SPARC-null CNS. At 2 d post ischemia, the number of PCNA-positive microglia in the lesioned cortex is significantly increased in SPARC nulls (Fig. 7*A*–C). SPARC may thus normally restrict the accumulation of microglia and macrophages in and around a focal ischemia lesion, but we do not know whether this is due directly to it impacting their proliferation or migration to the lesion site, or through a more indirect mechanism. To directly test if SPARC can regulate microglial proliferation, we used an *in vitro* assay. Microglia are traditionally harvested and cultured from perinatal mixed glial cultures. However, microglia derived from the early postnatal cortex (see Fig. 1) do not express SPARC *in vivo*, or, incidentally, *in vitro*, even if cultured for extended periods of time (Fig. 7*D*). SPARC is, however, expressed *in vitro* by GFAP-positive contaminating cells in postnatal cultures (data not shown). To obtain microglia that are more representative of their mature, "resting" phenotype (Santambrogio et al., 2001), microglia must be derived from adult mice following isolation using a discontinuous Percoll gradient, which highly enriches for mature isolectin IB4-positive microglia that also express SPARC, similar to adult microglia *in vivo* (Fig. 7*F*; 97% pure). Even under highly regulated *in vitro* conditions, SPARC expression is gradually lost as microglia are maintained over time *in vitro* (data not shown), in support of the belief that many microglia *in vitro* are not truly "resting." Detection of nuclear NFκB indicates that, even in the absence of inflammatory cytokine addition, subpopulations of microglia from early postnatal or mature cortex are similarly "partially activated" *in vitro* (Fig. 7 *D*,*E*). Following density gradient isolation, microglia derived from SPARC-null adult mice are initially morphologically similar to their wild-type counterparts, yet when seeded at the same density, they generate significantly more dense cultures after only DIV 8 (Fig. 7*F*,*G*). This increase in cell numbers is not due to a differential loss, but an increase in proliferation as demonstrated by thymidine analog incorporation. After DIV 2, SPARC-null adult-derived microglia showed significantly greater incorporation of EdU in a 48 h period, compared with microglia derived from wild-type mice (Fig. 7*H*), an enhanced proliferation that was partially reversed by adding exogenous SPARC in a dose-dependent manner.

Discussion

In this study, we have used a series of *in vitro* assays, analysis of spatiotemporal expression changes after two different lesions, and recovery analysis in double transgenic mice to test if SPARC

can directly regulate microglial responsiveness. SPARC is robustly induced by only mature, ramified microglia in the adult brain, but is lost from reactive hypertrophic or amoeboid microglia as they respond to both photothrombotic stroke and excitotoxic cortical lesion. When the CNS develops in the absence of SPARC, however, resting microglia become more abundant, and their branching is significantly more elaborate, with distinctly differential patterning in gray and white matter. Following photothrombotic stroke, cortical microgliosis is increased and functional recovery is enhanced in the absence of SPARC, thus SPARC appears to normally restrict microglial proliferation both *in vivo* and *in vitro*. These data suggest a potentially novel function of SPARC in regulating microglial patterning, proliferation, and response to lesion, and reveal a new pathway that could be temporally regulated to potentially alter the dynamics of the neuroimmune repair response.

During early postnatal development, SPARC is not expressed by developing microglia (monocytes) as they infiltrate into the CNS, proliferate, and migrate to their mature CNS location, and is only induced as microglia become mature and ramified (Fig. 1). In accord with this, when we prepare microglia derived from postnatal mixed glial cultures (using widely published techniques), they do not express SPARC, suggesting that they may not have yet attained full maturity. This alone is not novel—microglia from neonatal animals are known to be phenotypically different from microglia from adult rodents—but the majority of markers that differentiate their phenotype are linked to cytokine or chemokine signaling, not interaction with the ECM of the gray or white matter of the mature CNS. Neonatal microglia are not only functionally immature, but they have a "partially activated" phenotype (Carson et al., 1998; Santambrogio et al., 2001). Thus, SPARC expression appears indicative of a more mature "surveying" ramified phenotype, and is correspondingly lost after lesion *in vivo*, as resting microglia switch into a highly activated state (Figs. 1, 2).

Although most dynamic microglial "markers" suggest distinct heterogeneity of regional subpopulations of microglia, microglial expression and retention of SPARC in steady state is consistent across the adult brain (Lawson et al., 1990; Carson et al., 2007). SPARC is a multimodal protein that functions in a highly context-dependent manner. For example, different matrix metalloproteinases (MMPs) can cleave and make it shift activity to differentially bind to different ECM components, and SPARC can, in turn, regulate MMP production and activity. It is thus possible that microglial SPARC may play different roles in different regions of the CNS, and in different time windows after a lesion. For example, a novel developmental role for astrocyte-derived SPARC as a regulator of synapse formation and stabilization in early postnatal development has recently been elucidated (Jones et al., 2011; Kucukdereli et al., 2011). However, after P14, cortical and hippocampal astrocytes rarely express SPARC and when they do, it appears restricted to blood– brain barrier end feet. Given the recently demonstrated essential role of microglia in synaptic pruning during development (Paolicelli et al., 2011) and plasticity (Tremblay and Majewska, 2011), we show here that SPARC-expressing microglia are ideally situated throughout the gray matter to step in for astrocytes in this role in the adult CNS, and could also use SPARC as part of their molecular arsenal for modulating plasticity depending on the immune state of the CNS or periphery.

Following lesion, SPARC is lost in reactive and phagocytic microglia in and adjacent to the lesion site, but upregulated in reactive astrocytes and blood vessels demarcating the perilesion boundary of both ischemic and excitotoxic lesion cores (Figs. 2, 3, 5, 6). Early after lesion, some secreted SPARC appears diffusely distributed through the extracellular milieu of the lesion core. Here, by modulating local matrix and cytokine availability, it could have a more extensive localized impact on immune-mediated tissue remodeling that is quite different from its astrocytic role in modulating cell responses in the lesion penumbra. The upregulation of SPARC in perilesion reactive astrocytes here is consistent with other lesions, including cortical stab wound (Mendis et al., 1998), entorhinal deafferentation (Liu et al., 2005), spinal cord injury, and glial tumors (Capper et al., 2010). The spatiotemporal changes in SPARC expression that differ between these scenarios, however, suggest that SPARC may have different roles depending on the type, and extent, of lesion. The two lesions used here (Figs. 2, 3) suggest that the downregulation and rapid loss of SPARC (presumably by secretion into the lesion) is a consistent feature of microglia's phagocytic transformation. In addition, as phagocytic microglia begin to clear the lesion of debris, perilesion astrocytes upregulating SPARC could make it available to contribute to the significant later structural changes (e.g., scar formation and synaptic remodeling) that are observed in the perilesion zone following ischemia (Brown et al., 2007, 2010).

Using the CX3CR1-GFP reporter in a SPARC-null background allowed us to establish that even at rest, SPARC-null microglia extend more elaborate processes and display different patterns of branching, with significant and distinct differences between gray and white matter (Fig. 4). Preliminary live slice imaging of hippocampal slices prepared from CX3CR1-GFP/SPARC-null mice suggested that, despite their altered morphology, cortical and hippocampal microglia can still initially dynamically survey their environment successfully in the absence of SPARC (B. MacVicar, unpublished data). The double transgenic/null line was also critical to establish that SPARC regulates the spread of microgliosis *in vivo* following lesion (Fig. 6), even if the lesion volume of SPARC nulls is statistically indistinguishable from controls (Fig. 5). The antiproliferative activity of SPARC on microglia *in vivo* (Fig. 6) and *in vitro* (Fig. 7) is consistent with altered immune responses to CNS lesion in the absence of SPARC (Sangaletti et al., 2005, 2011; Au et al., 2007; Rempel et al., 2007). These findings also extend SPARC's reported antiproliferative activity in a number of nonimmune cells, like smooth muscle and endothelia (Raines et al., 1992; Sage et al., 1995), into the CNS. Ramified microglia represent a very stable cell population with a slow turnover (Lawson 1992).

It is possible that SPARC acts to maintain microglia in a stable, nonproliferative state by minimizing the microglial response to growth factors and local ECM. Both vascular endothelial growth factor and insulin-like growth factor 1 are released in the vicinity of a lesion, and can stimulate microglial proliferation (Forstreuter et al., 2002; O'Donnell et al., 2002), but are inhibited by SPARC (Kupprion et al., 1998; Francki et al., 2003). Furthermore, transforming growth factor β-1, whose activity is augmented by SPARC, inhibits microglial proliferation (Suzumura et al., 1993; Francki et al., 2004). Thus, SPARC could normally act as a modulator of ECM and growth factor interactions within a highly localized microglial microenvironment, and only when the external stimulus is beyond the threshold of SPARC's modulatory action (e.g., after lesion), can microglia undergo transformation into a hypertrophic, reactive state. Once activated, microglia then rapidly secrete their SPARC, stimulating a feedforward, rapid expansion of highly localized microglial populations.

The spatiotemporal changes in SPARC expression reported here support the hypothesis that SPARC could play different roles depending on the lesion scenario, and the loss of microglial SPARC may be an important trigger allowing proliferation of microglia following injury. The concurrent upregulation of SPARC in reactive astrocytes could be similarly intended to keep astrocytic scar proliferation in check, given that SPARC negatively correlates with proliferation in astrocytic tumors (Capper et al., 2010). However, reactive gliosis can also be protective following focal brain ischemia (Järlestedt et al., 2010), so this is unlikely to represent the whole picture. This immediate loss of microglial SPARC after lesion could also facilitate migration of other immune cells into the lesion core through SPARC's antiadhesive properties with ECM (Murphy-Ullrich, 2001) and also by regulating MMP expression and activity in the lesion environment (Rich et al., 2003; Kunigal et al., 2006; Said et al., 2007). The differences in behavioral recovery that emerge after the initial microgliosis (and are independent of lesion volume change) argue that these later activities induced by expanded microglia may be responsible for enhanced cortical function.

We thus reveal a novel role for SPARC as a glia-derived protein involved in regulation of the neuroimmune microglial response, and that its activity in repair may differ between gray and white matter. Manipulating the proliferation of microglia and macrophages following injury can be a double-edged sword, however. It is clear that preventing aberrant microglial proliferation could be highly desirable in some lesion scenarios, because activated microglia can themselves be neurotoxic (Walter and Neumann, 2009). However, it is also important that the immune response be initiated in a timely manner in the case of injury or disease. Selective ablation of proliferating microglia can exacerbate ischemic injury (Lalancette-Hébert et al., 2007), whereas here, functional recovery (in the absence of SPARC) is enhanced by increased microgliosis. The reactive state of microglia close to a CNS lesion must therefore be highly tuned, and here we present SPARC as a novel modulator of this crucial regulatory process. Controlling localized SPARC action may thus be a potential therapeutic avenue to modulate local neuroimmune responses, at the same time as carefully considering the other beneficial roles it may play in vascular and astrocytic remodeling at the perilesion boundary.

References

Au E, Richter MW, Vincent AJ, Tetzlaff W, Aebersold R, Sage EH, Roskams AJ (2007) SPARC from olfactory ensheathing cells stimulates Schwann cells to promote neurite outgrowth and enhances spinal cord repair. J Neurosci 27:7208–7221. CrossRef Medline

Basu A, Kligman LH, Samulewicz SJ, Howe CC (2001) Impaired wound healing in mice deficient in a matricellular protein SPARC (osteonectin, BM-40). BMC Cell Biol 2:15. CrossRef Medline

Bradshaw AD, Reed MJ, Sage EH (2002) SPARC-null mice exhibit accelerated cutaneous wound closure. J Histochem Cytochem 50:1–10. CrossRef Medline

Brekken RA, Sage EH (2001) SPARC, a matricellular protein: at the crossroads of cell-matrix communication. Matrix Biol 19:816–827. Medline

Brown CE, Li P, Boyd JD, Delaney KR, Murphy TH (2007) Extensive turnover of dendritic spines and vascular remodeling in cortical tissues recovering from stroke. J Neurosci 27:4101–4109. CrossRef Medline

Brown CE, Boyd JD, Murphy TH (2010) Longitudinal in vivo imaging reveals balanced and branch-specific remodeling of mature cortical pyramidal dendritic arbors after stroke. J Cereb Blood Flow Metab 30:783–791. CrossRef Medline

Capper D, Mittelbronn M, Goeppert B, Meyermann R, Schittenhelm J (2010) Secreted protein, acidic and rich in cysteine (SPARC) expression in astrocytic tumour cells negatively correlates with proliferation, while vascular SPARC expression is associated with patient survival. Neuropathol Appl Neurobiol 36:183–197. CrossRef Medline

Carson MJ, Reilly CR, Sutcliffe JG, Lo D (1998) Mature microglia resemble immature antigen-presenting cells. Glia 22:72–85. CrossRef Medline

Carson MJ, Bilousova TV, Puntambekar SS, Melchior B, Doose JM, Ethell IM (2007) A rose by any other name? The potential consequences of microglial heterogeneity during CNS health and disease. Neurotherapeutics 4:571–579. CrossRef Medline

Chan WY, Kohsaka S, Rezaie P (2007) The origin and cell lineage of microglia: new concepts. Brain Res Rev 53:344–354. CrossRef Medline

Clark DL, Penner M, Orellana-Jordan IM, Colbourne F (2008) Comparison of 12, 24 and 48 h of systemic hypothermia on outcome after permanent focal ischemia in rat. Exp Neurol 212:386–392. CrossRef Medline

Forstreuter F, Lucius R, Mentlein R (2002) Vascular endothelial growth factor induces chemotaxis and proliferation of microglial cells. J Neuroimmunol 132:93–98. CrossRef Medline

Francki A, Motamed K, McClure TD, Kaya M, Murri C, Blake DJ, Carbon JG, Sage EH (2003) SPARC regulates cell cycle progression in mesangial cells via its inhibition of IGF-dependent signaling. J Cell Biochem 88:802–811. CrossRef Medline

Francki A, McClure TD, Brekken RA, Motamed K, Murri C, Wang T, Sage EH (2004) SPARC regulates TGF-beta1-dependent signaling in primary glomerular mesangial cells. J Cell Biochem 91:915–925. CrossRef Medline

Gongidi V, Ring C, Moody M, Brekken R, Sage EH, Rakic P, Anton ES (2004) SPARC-like 1 regulates the terminal phase of radial glia-guided migration in the cerebral cortex. Neuron 41:57–69. CrossRef Medline

Iadecola C, Anrather J (2011) The immunology of stroke: from mechanisms to translation. Nat Med 17:796–808. CrossRef Medline

Järlestedt K, Rousset CI, Faiz M, Wilhelmsson U, Ståhlberg A, Sourkova H, Pekna M, Mallard C, Hagberg H, Pekny M (2010) Attenuation of reactive gliosis does not affect infarct volume in neonatal hypoxic-ischemic brain injury in mice. PLoS One 5:e10397. CrossRef Medline

Jones EV, Bernardinelli Y, Tse YC, Chierzi S, Wong TP, Murai KK (2011) Astrocytes control glutamate receptor levels at developing synapses through SPARC-beta-integrin interactions. J Neurosci 31:4154–4165. CrossRef Medline

Jung S, Aliberti J, Graemmel P, Sunshine MJ, Kreutzberg GW, Sher A, Littman DR (2000) Analysis of fractalkine receptor CX(3)CR1 function by targeted deletion and green fluorescent protein reporter gene insertion. Mol Cell Biol 20:4106–4114. CrossRef Medline

Kucukdereli H, Allen NJ, Lee AT, Feng A, Ozlu MI, Conatser LM, Chakraborty C, Workman G, Weaver M, Sage EH, Barres BA, Eroglu C (2011) Control of excitatory CNS synaptogenesis by astrocyte-secreted proteins Hevin and SPARC. Proc Natl Acad Sci U S A 108:E440–E449. CrossRef Medline

Kunigal S, Gondi CS, Gujrati M, Lakka SS, Dinh DH, Olivero WC, Rao JS (2006) SPARC-induced migration of glioblastoma cell lines via uPA-uPAR signaling and activation of small GTPase RhoA. Int J Oncol 29:1349–1357. Medline

Kupprion C, Motamed K, Sage EH (1998) SPARC (BM-40, osteonectin) inhibits the mitogenic effect of vascular endothelial growth factor on microvascular endothelial cells. J Biol Chem 273:29635–29640. CrossRef Medline

Lalancette-Hébert M, Gowing G, Simard A, Weng YC, Kriz J (2007) Selective ablation of proliferating microglial cells exacerbates ischemic injury in the brain. J Neurosci 27:2596–2605. CrossRef Medline

Lawson LJ, Perry VH, Dri P, Gordon S (1990) Heterogeneity in the distribution and morphology of microglia in the normal adult mouse brain. Neuroscience 39:151–170. CrossRef Medline

Lawson LJ, Perry VH, Gordon S (1992) Turnover of resident microglia in the normal adult mouse brain. Neuroscience 48:405–415. CrossRef Medline

Liu X, Ying G, Wang W, Dong J, Wang Y, Ni Z, Zhou C (2005) Entorhinal deafferentation induces upregulation of SPARC in the mouse hippocampus. Brain Res Mol Brain Res 141:58–65. CrossRef Medline

Lloyd-Burton S, Roskams AJ (2012) AJ SPARC Like-1 (SC1) is a diversely expressed and developmentally regulated matricellular protein that does not compensate for the absence of SPARC in the CNS. J Comp Neurol 520:2575–2590. CrossRef Medline

Mendis DB, Ivy GO, Brown IR (1998) SPARC/osteonectin mRNA is induced in blood vessels following injury to the adult rat cerebral cortex. Neurochem Res 23:1117–1123. CrossRef Medline

Moskowitz MA, Lo EH, Iadecola C (2010) The science of stroke: mechanisms in search of treatments. Neuron 67:181–198. CrossRef Medline

Murphy-Ullrich JE (2001) The de-adhesive activity of matricellular proteins: is intermediate cell adhesion an adaptive state? J Clin Invest 107: 785–790. CrossRef Medline

Nimmerjahn A, Kirchhoff F, Helmchen F (2005) Resting microglial cells are highly dynamic surveillants of brain parenchyma in vivo. Science 308: 1314–1318. CrossRef Medline

O'Donnell SL, Frederick TJ, Krady JK, Vannucci SJ, Wood TL (2002) IGF-I and microglia/macrophage proliferation in the ischemic mouse brain. Glia 39:85–97. CrossRef Medline

Paolicelli RC, Bolasco G, Pagani F, Maggi L, Scianni M, Panzanelli P, Giustetto M, Ferreira TA, Guiducci E, Dumas L, Ragozzino D, Gross CT (2011) Synaptic pruning by microglia is necessary for normal brain development. Science 333:1456–1458. CrossRef Medline

Porritt MJ, Andersson HC, Hou L, Nilsson Å, Pekna M, Pekny M, Nilsson M (2012) "Photothrombosis-induced infarction of the mouse cerebral cortex is not affected by the Nrf2-activator sulforaphane. PLoS One 7:e41090. CrossRef Medline

Raines EW, Lane TF, Iruela-Arispe ML, Ross R, Sage EH (1992) The extracellular glycoprotein SPARC interacts with platelet-derived growth factor (PDGF)-AB and -BB and inhibits the binding of PDGF to its receptors. Proc Natl Acad Sci U S A 89:1281–1285. CrossRef Medline

Ransohoff RM, Cardona AE (2010) The myeloid cells of the central nervous system parenchyma. Nature 468:253–262. CrossRef Medline

Rempel SA, Hawley RC, Gutiérrez JA, Mouzon E, Bobbitt KR, Lemke N, Schultz CR, Schultz LR, Golembieski W, Koblinski J, VanOsdol S, Miller CG (2007) Splenic and immune alterations of the Sparc-null mouse accompany a lack of immune response. Genes Immun 8:262–274. CrossRef Medline

Rich JN, Shi Q, Hjelmeland M, Cummings TJ, Kuan CT, Bigner DD, Counter CM, Wang XF (2003) Bone-related genes expressed in advanced malignancies induce invasion and metastasis in a genetically defined human cancer model. J Biol Chem 278:15951–15957. CrossRef Medline

Sage EH, Bassuk JA, Yost JC, Folkman MJ, Lane TF (1995) Inhibition of endothelial cell proliferation by SPARC is mediated through a Ca(2+)-binding EF-hand sequence. J Cell Biochem 57:127–140. CrossRef Medline

Said N, Socha MJ, Olearczyk JJ, Elmarakby AA, Imig JD, Motamed K (2007) Normalization of the Ovarian Cancer Microenvironment by SPARC. Mol Cancer Res 5:1015–1030. CrossRef Medline

Sangaletti S, Gioiosa L, Guiducci C, Rotta G, Rescigno M, Stoppacciaro A, Chiodoni C, Colombo MP (2005) Accelerated dendritic-cell migration and T-cell priming in SPARC-deficient mice. J Cell Sci 118:3685–3694. CrossRef Medline

Sangaletti S, Tripodo C, Cappetti B, Casalini P, Chiodoni C, Piconese S, Santangelo A, Parenza M, Arioli I, Miotti S, Colombo MP (2011) SPARC oppositely regulates inflammation and fibrosis in bleomycin-induced lung damage. Am J Pathol 179:3000–3010. CrossRef Medline

Santambrogio L, Belyanskaya SL, Fischer FR, Cipriani B, Brosnan CF, Ricciardi-Castagnoli P, Stern LJ, Strominger JL, Riese R (2001) Developmental plasticity of CNS microglia. Proc Natl Acad Sci U S A 98:6295–6300. CrossRef Medline

Schallert T, Fleming SM, Leasure JL, Tillerson JL, Bland ST (2000) CNS plasticity and assessment of forelimb sensorimotor outcome in unilateral rat models of stroke, cortical ablation, parkinsonism and spinal cord injury. Neuropharmacology 39:777–787. CrossRef Medline

Schellings MW, van Almen GC, Sage EH, Heymans S (2009) Thrombospondins in the heart: potential functions in cardiac remodeling. J Cell Commun Signal 3:201–213. CrossRef Medline

Sultan-Styne K, Toledo R, Walker C, Kallkopf A, Ribak CE, Guthrie KM (2009) Long-term survival of olfactory sensory neurons after target depletion. J Comp Neurol 515:696–710. CrossRef Medline

Suzumura A, Sawada M, Yamamoto H, Marunouchi T (1993) Transforming growth factor-beta suppresses activation and proliferation of microglia in vitro. J Immunol 151:2150–2158. Medline

Tremblay MÉ, Majewska AK (2011) A role for microglia in synaptic plasticity? Commun Integr Biol 4:220–222. CrossRef Medline

Vergara-Aragon P, Gonzalez CL, Whishaw IQ (2003) A novel skilled-reaching impairment in paw supination on the "good" side of the hemi-Parkinson rat improved with rehabilitation. J Neurosci 23:579–586. Medline

Vincent AJ, Lau PW, Roskams AJ (2008) SPARC is expressed by macroglia and microglia in the developing and mature nervous system. Dev Dyn 237:1449–1462. CrossRef Medline

Walter L, Neumann H (2009) Role of microglia in neuronal degeneration and regeneration. Semin Immunopathol 31:513–525. CrossRef Medline

Walther M, Kuklinski S, Pesheva P, Guntinas-Lichius O, Angelov DN, Neiss WF, Asou H, Probstmeier R (2000) Galectin-3 is upregulated in microglial cells in response to ischemic brain lesions, but not to facial nerve axotomy. J Neurosci Res 61:430–435. CrossRef Medline

Watson BD, Dietrich WD, Busto R, Wachtel MS, Ginsberg MD (1985) Induction of reproducible brain infarction by photochemically initiated thrombosis. Ann Neurol 17:497–504. CrossRef Medline

Yan YP, Lang BT, Vemuganti R, Dempsey RJ (2009) Galectin-3 mediates postischemic tissue remodeling. Brain Res 1288:116–124. CrossRef Medline

Zhang W, Xie Y, Wang T, Bi J, Li H, Zhang LQ, Ye SQ, Ding S (2010) Neuronal protective role of PBEF in a mouse model of cerebral ischemia. J Cereb Blood Flow Metab 30:1962–1971. CrossRef Medline